CrystEngComm

PAPER

View Article Online
View Journal | View Issue

Cite this: *CrystEngComm*, 2014, **16**, 3203

Syntheses, structures, and magnetic properties of five coordination polymers constructed from biphenyl-3,4′,5-tricarboxylic acid and (bis)imidazole linkers†

Xiutang Zhang,*[ab] Liming Fan,[ab] Wei Zhang,[a] Weiliu Fan,[b] Liming Sun[b] and Xian Zhao*[b]

Five coordination polymers (CPs), namely $\{[Ni_{1.5}(BPT)(1,4\text{-bib})_2(H_2O)]\cdot(1,4\text{-bib})_{0.5}\cdot 2H_2O\}_n$ (**1**), $\{[Co_2(BPT)(1,3\text{-bimb})(\mu_3\text{-OH})]\cdot H_2O\}_n$ (**2**), $\{[Zn(HBPT)(1,3\text{-bimb})]\cdot H_2O\}_n$ (**3**), $\{[Co_2(BPT)(H_2BPT)(4,4'\text{-bibp})_2]\cdot 2H_2O\}_n$ (**4**), and $[Mn_{2.5}(BPT)(4,4'\text{-bibp})_{2.5}(SO_4)(H_2O)]_n$ (**5**) (H_3BPT = biphenyl-3,4′,5-tricarboxylic acid, 1,4-bib = 1,4-bis(1*H*-imidazol-1-yl)benzene, 1,3-bimb = 1,3-bis(imidazol-1-ylmethyl)benzene, and 4,4′-bibp = 4,4′-bis(imidazol-1-yl)biphenyl), were synthesized under hydrothermal conditions. Their structures were determined by single-crystal X-ray diffraction analyses and further characterized by elemental analyses, IR spectroscopy, powder X-ray diffraction (PXRD), and thermogravimetric (TG) analyses. Complex **1** exhibits unprecedented 2D + 2D → 3D parallel entangled networks consisting of trilayer (3,4,6)-connected $(4^4\cdot5^4\cdot6^6\cdot8)(5\cdot6^4\cdot8)_2(5^2\cdot6^2)$ sheets. Complex **2** displays a 3D (3,10)-connected 3,10T9 net based on tetranuclear $\{Co_4(\mu_3\text{-OH})_2\}$ clusters with the Schläfli symbol $(4^{18}\cdot6^{24}\cdot8^3)(4^3)_2$. Complex **3** shows an interesting 1D tube-like chain consisting of $Zn_2(1,3\text{-bimb})_2$ loops. Complex **4** affords a 2D $(4^4\cdot6^2)$-sql net constructed from $\{Co_2\}$ dinuclear units. Complex **5** displays a 3D 6-connected $(4^{12}\cdot6^3)$-pcu net consisting of α-Po primitive cubic nets based on $\{Mn_5(SO_4)_2\}$ clusters. Moreover, magnetic studies indicate that complexes **2**, **4** and **5** show antiferromagnetic properties.

Received 17th December 2013,
Accepted 29th January 2014

DOI: 10.1039/c3ce42565g

www.rsc.org/crystengcomm

Introduction

Recent research into coordination polymers (CPs) has been attractive in the field of materials science due to their fascinating structures and new topological prototypes, as well as their tremendous potential applications as functional materials in gas storage and separation,[1] ion exchange,[2] luminescence,[3] magnetism,[4] photocatalysis,[5] and heterogeneous catalysis.[6] Up to now, much effort has been devoted and a large number of CPs with various architectures and excellent properties have been obtained through the self-assembly of selected or various designed organic ligands and metal ions or metal–oxide building units.

However, the controllable synthesis of prospective networks is still a far-reaching challenge since such materials are always dependent on many uncertain factors, such as the coordination geometry preferred by the metal,[7] solvent systems,[8] templates,[9] pH values,[10] counteranions,[11] and the chemical structures of the selected ligands.[12] Among these factors, the rational selection of the characteristic ligand proved to be one efficient route for the construction of versatile CPs. Generally, the length, rigidity, coordination modes, and functional groups or substituents of polycarboxylate ligands have consequential effects on the final structures of CPs.[13] Moreover, a recent study on coordination assemblies using (bis)imidazole linkers as ancillary ligands provided a reliable strategy for obtaining new topological prototypes of coordination nets.[14] The ancillary ligands have a great effect on the coordination modes of the host polycarboxylate aromatic acid and the final packing structures. With the length of the ancillary ligands increasing, the longer separation of neighboring central ions makes the host aromatic polycarboxylate ligand adopt more "open" coordination modes and the overall structure a higher degree of interpenetration. The greater flexibility of ancillary ligands could make the final structure more twisted and complicated.[15] Thus, CPs

[a] *Advanced Material Institute of Research, College of Chemistry and Chemical Engineering, Qilu Normal University, Jinan, 250013, China. E-mail: xiutangzhang@163.com*
[b] *State Key Laboratory of Crystal Materials, Shandong University, Jinan 250100, China. E-mail: zhaoxian@icm.sdu.edu.cn*

† Electronic supplementary information (ESI) available: Additional figures, IR spectra, powder XRD patterns and X-ray crystallographic data. CCDC 977304–977308 for **1**–**5**. For ESI and crystallographic data in CIF or other electronic format see DOI: 10.1039/c3ce42565g

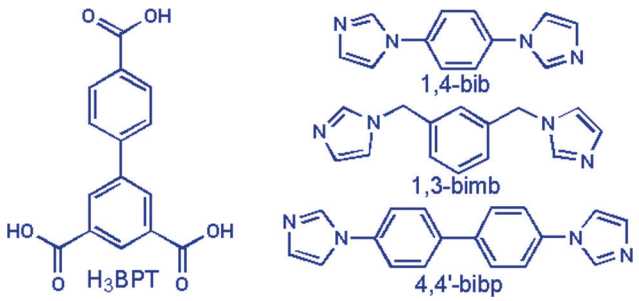

Scheme 1 Structures of H_3BPT and three bis(imidazole) bridging ligands.

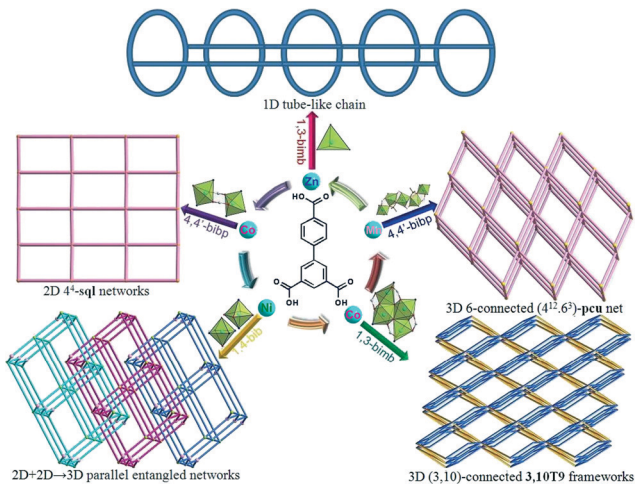

Scheme 2 Various structures of complexes **1**–**5**.

can be assembled from predetermined organic building blocks through judicious selection of ligands and careful control of reaction conditions. To the best of our knowledge, CPs based on biphenyl-3,4′,5-tricarboxylic acid (H_3BPT) in the presence of (bis)imidazole linkers have never been documented to date.

Thus, these considerations inspired us to explore new coordination frameworks with biphenyl-3,4′,5-tricarboxylic acid (H_3BPT) and bis(imidazole) bridging linkers (1,4-bib, 1,3-bimb, and 4,4′-bibp, Scheme 1). Herein, we reported the syntheses and structural characterization of five new coordination polymers, $\{[Ni_{1.5}(BPT)(1,4\text{-bib})_2(H_2O)]\cdot(1,4\text{-bib})_{0.5}\cdot 2H_2O\}_n$ (**1**), $\{[Co_2(BPT)(1,3\text{-bimb})(\mu_3\text{-OH})]\cdot H_2O\}_n$ (**2**), $\{[Zn(HBPT)(1,3\text{-bimb})]\cdot H_2O\}_n$ (**3**), $\{[Co_2(BPT)(H_2BPT)(4,4'\text{-bibp})_2]\cdot 2H_2O\}_n$ (**4**), and $[Mn_{2.5}(BPT)(4,4'\text{-bibp})_{2.5}(SO_4)(H_2O)]_n$ (**5**), which exhibit a systematic variation of architectures from a 1D ladder chain to a 3D framework (Scheme 2) constructed from H_3BPT and three bis(imidazole) bridging linkers (1,4-bib, 1,3-bimb, and 4,4′-bibp). Magnetic studies indicate that complexes of **2**, **4**, and **5** show antiferromagnetic behavior.

Experimental section

Materials and physical measurements

All chemicals were purchased from Jinan Henghua Sci. & Tec. Co. Ltd. and used without further purification. IR spectra were measured using a Nicolet 740 FTIR spectrometer at the range of 400–4000 cm^{-1}. Elemental analyses were carried out using a CE instruments EA 1110 elemental analyzer. X-ray powder diffraction peaks were measured using a PANalytical X-Pert pro diffractometer with Cu-Kα radiation. Thermogravimetric analyses (TGA) were performed under air conditions from room temperature to 800 °C with a heating rate of 10 °C min^{-1} using a Perkin-Elmer TGA-7 thermogravimetric analyzer. The magnetic measurements were made using Quantum Design SQUID MPMS XL-7 instruments.

Synthesis of $\{[Ni_{1.5}(BPT)(1,4\text{-bib})_2(H_2O)]\cdot(1,4\text{-bib})_{0.5}\cdot 2H_2O\}_n$ (1)

A mixture of H_3BPT (0.15 mmol, 0.043 g), 1,4-bib (0.20 mmol, 0.042 g), $NiSO_4\cdot 6H_2O$ (0.20 mmol, 0.053 g), NaOH (0.30 mmol, 0.012 g), and 12 mL H_2O was placed in a 25 mL Teflon-lined stainless steel vessel and heated to 170 °C for 3 days, followed by slow cooling (a descent rate of 10 °C h^{-1}) to room temperature. The green block crystals of **1** were obtained. Yield: 53% (based on Ni). Anal. (%) calcd. for $C_{90}H_{76}N_{20}Ni_3O_{18}$ (1901.84): C, 56.84; H, 4.03; N, 14.73. Found: C, 56.93; H, 3.76; N, 14.15. IR (KBr pellet, cm^{-1}): 3405 (m), 1603 (m), 1517 (s), 1387 (s), 1319 (m), 1074 (m), 831 (m), 713 (w).

Synthesis of $\{[Co_2(BPT)(1,3\text{-bimb})(\mu_3\text{-OH})]\cdot H_2O\}_n$ (2)

A mixture of H_3BPT (0.15 mmol, 0.043 g), 1,3-bimb (0.20 mmol, 0.048 g), $Co(NO_3)\cdot 6H_2O$ (0.20 mmol, 0.058 g), NaOH (0.30 mmol, 0.012 g), and 12 mL H_2O was placed in a 25 mL Teflon-lined stainless steel vessel and heated to 170 °C for 3 days, followed by slow cooling (a descent rate of 10 °C h^{-1}) to room temperature. The red block crystals of **2** were obtained. Yield: 47% (based on Co). Anal. (%) calcd. for $C_{29}H_{24}Co_2N_4O_8$ (674.38): C, 51.65; H, 3.59; N, 8.31. Found: C, 51.43; H, 3.43; N, 8.77. IR (KBr pellet, cm^{-1}): 3467 (m), 1619 (s), 1596 (s), 1567 (s), 1398 (s), 1274 (w), 1087 (w), 978 (w), 836 (w), 722 (m).

Synthesis of $\{[Zn(HBPT)(1,3\text{-bimb})]\cdot H_2O\}_n$ (3)

A mixture of H_3BPT (0.20 mmol, 0.057 g), 1,3-bimb (0.20 mmol, 0.048 g), $ZnSO_4\cdot 7H_2O$ (0.30 mmol, 0.086 g), $(NH_4)_6Mo_7O_{24}\cdot 4H_2O$ (0.81 mmol, 0.100 g), NaOH (0.20 mmol, 0.008 g), and 15 mL H_2O was placed in a 25 mL Teflon-lined stainless steel vessel and heated to 170 °C for 3 days, followed by slow cooling (a descent rate of 10 °C h^{-1}) to room temperature. The colorless block crystals of **3** were obtained. Yield: 42% (based on Zn). Anal. (%) calcd. for $C_{29}H_{24}N_4O_7Zn$ (605.89): C, 57.48; H, 3.99; N, 9.25. Found: C, 57.89; H, 4.03; N, 9.38. IR (KBr pellet, cm^{-1}): 3469 (m), 1621 (s), 1536 (s), 1394 (s), 1284 (w), 1109 (m), 944 (w), 778 (w), 730 (m).

Synthesis of $\{[Co_2(BPT)(H_2BPT)(4,4'\text{-bibp})_2]\cdot 2H_2O\}_n$ (4)

A mixture of H_3BPT (0.15 mmol, 0.043 g), 4,4′-bibp (0.40 mmol, 0.114 g), $Co(NO_3)\cdot 6H_2O$ (0.40 mmol, 0.116 g), NaOH (0.30 mmol, 0.012 g), and 12 mL H_2O was placed in a 25 mL Teflon-lined stainless steel vessel and heated to 170 °C for 3 days, followed by slow cooling (a descent rate of 10 °C h^{-1}) to room temperature. The red block crystals of **4** were obtained. Yield: 47%

Table 1 Crystal data for 1–5[a]

Compound	1	2	3	4	5
Empirical formula	$C_{90}H_{76}N_{20}Ni_3O_{18}$	$C_{29}H_{24}Co_2N_4O_8$	$C_{29}H_{24}N_4O_7Zn$	$C_{67}H_{49}Co_2N_8O_{14}$	$C_{120}H_{88}Mn_5N_{20}O_{22}S_2$
Formula weight	1901.84	674.38	605.89	1308.00	2500.92
Crystal system	Triclinic	Monoclinic	Triclinic	Monoclinic	Triclinic
Space group	$P\bar{1}$	$P2(1)/n$	$P\bar{1}$	$P2(1)$	$P\bar{1}$
a (Å)	13.4907(14)	12.337(2)	8.9151(10)	11.7332(4)	12.150(3)
b (Å)	13.5050(14)	11.051(2)	12.3303(13)	15.2259(6)	13.422(3)
c (Å)	13.7924(14)	21.819(4)	13.3052(14)	16.1433(6)	17.825(4)
α (°)	102.084(2)	90	108.564(2)	90	77.205(4)
β (°)	97.561(2)	100.761(4)	107.760(2)	102.4970(10)	70.985(4)
γ (°)	116.001(2)	90	99.002(2)	90	83.344(4)
V (Å^3)	2136.0(4)	2922.3(9)	1267.3(2)	2815.65(18)	2676.8(10)
Z	1	4	2	2	1
D_{calcd} (g cm^{-3})	1.479	1.533	1.588	1.543	1.551
μ (mm^{-1})	0.738	1.192	1.028	0.670	0.699
R_{int}	0.0168	0.0673	0.0420	0.0250	0.0342
Final R indices [$I > 2\sigma(I)$]	R_1 = 0.0464	R_1 = 0.0470	R_1 = 0.0450	R_1 = 0.0452	R_1 = 0.0690
	wR_2 = 0.1283	wR_2 = 0.0971	wR_2 = 0.1228	wR_2 = 0.1183	wR_2 = 0.1102
R indices (all data)	R_1 = 0.0582	R_1 = 0.0811	R_1 = 0.0574	R_1 = 0.0519	R_1 = 0.1185
	wR_2 = 0.1381	wR_2 = 0.1138	wR_2 = 0.1378	wR_2 = 0.1237	wR_2 = 0.1581
Gof	1.003	1.001	0.997	1.002	1.000

[a] $R_1 = \sum||F_o| - |F_c||/\sum|F_o|$, $wR_2 = [\sum w(F_o^2 - F_c^2)^2]/\sum w(F_o^2)^2]^{1/2}$.

(based on Co). Anal. (%) calcd. for $C_{67}H_{49}Co_2N_8O_{14}$ (1308.00): C, 61.52; H, 3.78; N, 8.57. Found: C, 61.21; H, 3.71; N, 8.69. IR (KBr pellet, cm^{-1}): 3431 (m), 3128 (m), 1605 (m), 1509 (s), 1382 (s), 1301 (s), 1060 (m), 814 (m), 658 (w).

Synthesis of $[Mn_{2.5}(BPT)(4,4'\text{-bibp})_{2.5}(SO_4)(H_2O)]_n$ (5)

The same synthesis procedure as for 4 was used except that $Co(NO_3)\cdot 6H_2O$ was replaced by $MnSO_4\cdot H_2O$, giving yellow block crystals. Yield: 43% (based on Mn). Anal. (%) calcd. for $C_{120}H_{88}Mn_5N_{20}O_{22}S_2$ (2500.92): C, 57.63; H, 3.55; N, 11.20. Found: C, 57.89; H, 3.72; N, 10.93. IR (KBr pellet, cm^{-1}): 3445 (m), 3123 (m), 1604 (s), 1509 (vs), 1291 (s), 1051 (s), 819 (s), 724 (w).

X-ray crystallography

Intensity data collection was carried out using a Siemens SMART diffractometer equipped with a CCD detector using Mo-Kα monochromatized radiation (λ = 0.71073 Å) at 293(2) or 296(2) K. The absorption correction was based on multiple and symmetry-equivalent reflections in the data set using the SADABS program based on the method of Blessing. The structures were solved by direct methods and refined by full-matrix least-squares using the SHELXTL package.[16] All non-hydrogen atoms were refined anisotropically. Hydrogen atoms except those of water molecules were generated geometrically with fixed isotropic thermal parameters and included in the structure factor calculations. The approximate positions of the water H atoms, obtained from a difference Fourier map, were restrained to the ideal configuration of the water molecules and fixed in the final stages of refinement. Four carbon atoms from one phenyl ring of BPT^{3-} in compound 1 are disordered and refined with an occupancy ratio of 40 : 60. For 1 and 4, there are some very large ADPs in the (bis)imidazole linkers. Crystallographic data for compounds 1–5 are given in Table 1. Selected bond lengths and angles are listed in Table S1.† Topological analysis of the coordination networks of all of the compounds was performed using the program package TOPOS.[17]

Results and discussion

Synthesis and general characterization

In the present study, complexes 1–5 were prepared from the solvothermal reaction of the related first transition metal salts and H_3BPT in the presence of rigid or flexible (bis)imidazole bridging linkers (1,4-bib, 1,3-bimb, and 4,4′-bibp). All of the complexes 1–5 are stable in the solid state upon extended exposure to air. They have poor solubility in water and common organic solvents but can be slightly soluble in very high polarity solvents.

Powder X-ray diffraction (PXRD) has been employed to check the phase purity of the bulk samples in the solid state. For complexes 1–5, the measured PXRD patterns closely match the simulated patterns generated from the results of single crystal diffraction, indicative of pure products (Fig. S1, ESI†). The absorption bands in the range of 3400–3500 cm^{-1} for 1–5 can be attributed to the characteristic peaks of water O–H vibrations. The vibrations at *ca.* 1520 and 1610 cm^{-1} correspond to the asymmetric and symmetric stretching vibrations of the carboxylate groups, respectively (Fig. S2†).

Structure descriptions of $\{[Ni_{1.5}(BPT)(1,4\text{-bib})_2(H_2O)]\cdot(1,4\text{-bib})_{0.5}\cdot 2H_2O\}_n$ (1)

The single-crystal X-ray diffraction analysis reveals that complex 1 crystallizes in the triclinic system, $P\bar{1}$ space group. As shown in Fig. 1a, there are one and a half of Ni^{II} ions, one

completely deprotonated BPT^{3-} ligand, two 1,4-bib ligands, one coordinated water molecule, and guest molecules including a half of 1,4-bib and two water molecules in the asymmetric unit. The Ni(1) cation is coordinated by four oxygen atoms from two BPT^{3-} ligands and one water molecule and two nitrogen atoms from two individual 1,4-bib ligands, resulting in a distorted octahedral geometry. Ni(2) is coordinated by two oxygen atoms from two BPT^{3-} ligands and two nitrogen atoms from two 1,4-bib ligands. The bond lengths of Ni–O and Ni–N are in the range of 1.9968(18)–2.1957(17) Å and 2.053(2)–2.121(2) Å, respectively. The ligand of BPT^{3-} exhibits a $(\kappa^0\text{-}\kappa^1)\text{-}(\kappa^0\text{-}\kappa^1)\text{-}(\kappa^1\text{-}\kappa^1)\text{-}\mu_3$ coordination mode (Mode I, Scheme 3) and connects three Ni^{II} ions to form a 1D $[Ni_3(BPT)_2]_n$ ladder chain (Fig. S3†).

Ni(1) ions are linked by 1,4-bib ligands to form a 2D $[Ni(1,4\text{-bib})_2]_n$ net along the *bc* plane (Fig. S4†). Above and below the $[Ni(1,4\text{-bib})_2]_n$ layer, two other layers are constructed from the mixed ligands of 1,4-bib and BPT^{3-}. These three coordination planes are further linked through the $(\kappa^1\text{-}\kappa^0)\text{-}\mu_1$ carboxyl groups, generating a 2D network containing a cavity with dimensions of 13.505(0) × 13.792(4) × 18.380(9) $Å^3$ (Fig. 1b). The 2D networks are further connected with each other, finally resulting in a 2D + 2D → 3D parallel framework (Fig. 1c). It is noteworthy that the guest molecules (1,4-bib and H_2O) occupied the channels *via* hydrogen bonds, which may be one important factor to stabilize the whole framework. Further, PLATON[18] calculated the void volume of **1** to be 1.8% (38.2 out of the 2136.0 $Å^3$ unit cell volume).

The topology analysis shows that the overall framework of complex **1** can be described as a trinodal (3,4,6)-connected net with the point symbol $(4^4{\cdot}5^4{\cdot}6^6{\cdot}8)(5{\cdot}6^4{\cdot}8)_2(5^2{\cdot}6^2)$ by denoting BPT^{3-}, Ni(1), and Ni(2) as 3-connected, 6-connected, and 4-connected nodes, respectively (Fig. 1d).

Structure descriptions of $\{[Co_2(BPT)(1,3\text{-bimb})(\mu_3\text{-OH})]{\cdot}H_2O\}_n$ (2)

The application of 1,3-bimb during the synthesis of **2**, which is more flexible and longer than 1,4-bib applied in complex **1**, resulted in a 3D high connected framework consisting of the $[Co_4(\mu_3\text{-OH})_2]^{6+}$ tetrameric SBUs in **2**. This proves that, with the length and flexibility of the ancillary ligands increasing, the longer separation of neighboring central ions makes the host aromatic polycarboxylate ligand adopt more "open" coordination modes and the overall structure exhibits a higher degree of interpenetration.[15c]

Complex **2** crystallizes in the monoclinic system, $P2_1/n$ space group. The asymmetric unit of complex **2** consists of two Co^{II} ions, one BPT^{3-} ligand, one 1,3-bimb ligand, one $\mu_3\text{-}OH^-$ anion, and one lattice water molecule (Fig. 2a). Four Co^{II} ions are connected through μ_3-OH, giving a

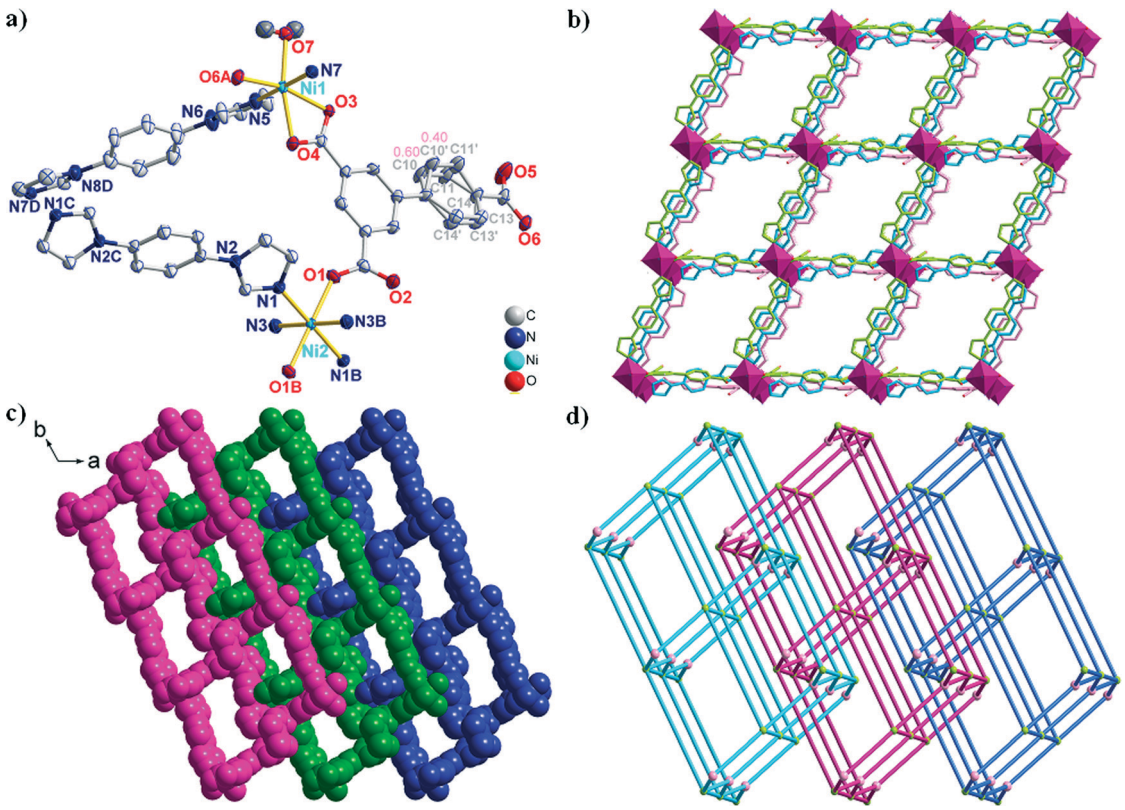

Fig. 1 (a) ORTEP representation of **1** with 50% thermal ellipsoid probability. Guest molecules and hydrogen atoms are omitted for clarity. Symmetry codes: A: *x*, *y*, −1 + *z*; B: 2 − *x*, 1 − *y*, 1 − *z*; C: 2 − *x*, 1 − *y*, −*z*; D: *x*, 1 + *y*, *z*. (b) The unprecedented $Ni_2(BPT)(1,4\text{-bib})_2$ trilayer. (c) The 2D + 2D → 3D parallel entangled networks viewed along the *c* axis. (d) The 2D + 2D → 3D interpenetrated (3,4,6)-connected topology $(4^4{\cdot}5^4{\cdot}6^6{\cdot}8)(5{\cdot}6^4{\cdot}8)_2(5^2{\cdot}6^2)$ sheets in **1**.

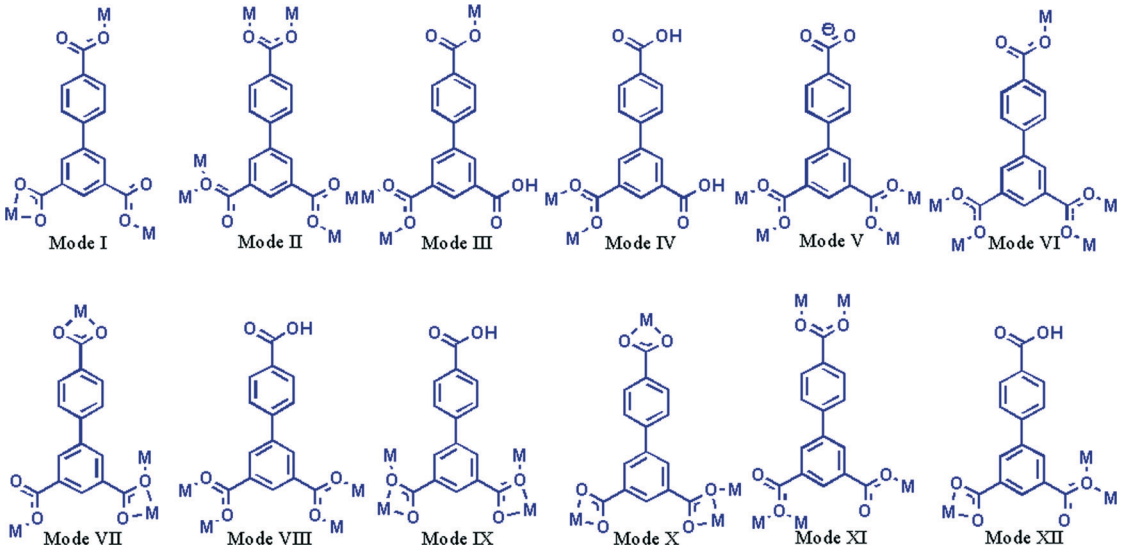

Scheme 3 The coordination modes of H_3BPT in complexes **1**–**5**.

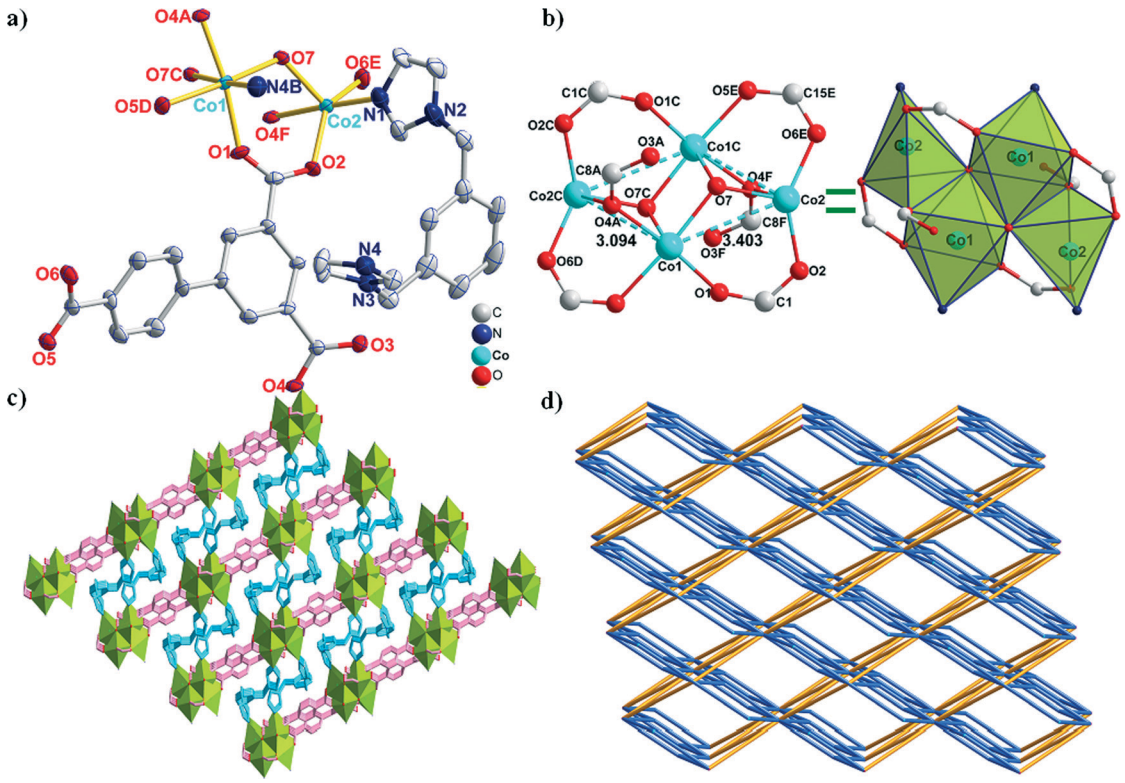

Fig. 2 (a) ORTEP representation of **2** with 50% thermal ellipsoid probability. Hydrogen atoms are omitted for clarity. Symmetry codes: A: *x*, 1 + *y*, *z*; B: 1.5 − *x*, 0.5 + *y*, 0.5 − *z*; C: 2 − *x*, 2 − *y*, 1 − *z*; D: 2.5 − *x*, 0.5 + *y*, 0.5 − *z*; E: −0.5 + *x*, 1.5 − *y*, 0.5 + *z*; F: 2 − *x*, 1 − *y*, 1 − *z*. (b) The $Co_4(COO)_6(\mu_3\text{-}OH)_2$ SBUs in **2**. (c) A perspective view of the 3D frameworks viewed along the *b* axis. (d) The 3D (3,10)-connected 3,10T9 topology with the Schläfli symbol $(4^{18}{\cdot}6^{24}{\cdot}8^3)_2$ in **2**.

parallelogram $[Co_4(\mu_3\text{-}OH)_2]^{6+}$ tetrameric SBU with Co⋯Co distances of 3.403 Å and 3.094 Å (Fig. 2b). Co(1) is located in a distorted octahedral $\{CoO_5N\}$ geometry, coordinated by three carboxylate oxygen atoms from three BPT^{3-} ligands, two μ_3-OH oxygen atoms, and one nitrogen atom from a 1,4-bib ligand, whereas Co(2) is located in a distorted trigonal bipyramidal CoO_4N geometry, coordinated by four carboxylate oxygen atoms from three different BPT^{3-} ligands and one μ_3-OH, and one nitrogen atom from one 1,3-bimb ligand. The Co–O bond lengths are in the range of 1.968(3)–2.253(3) Å, and the Co–N bond distances are 2.057(4) and 2.114(3) Å, respectively.

The BPT^{3-} ligand exhibits an unreported $(\kappa^1\text{-}\kappa^1)\text{-}(\kappa^1\text{-}\kappa^1)\text{-}(\kappa^0\text{-}\kappa^2)\text{-}\mu_6$ coordination mode (Mode II) linking the $[Co_4(\mu_3\text{-}OH)_2]^{6+}$ tetrameric SBUs, finally resulting in a 2D $[Co_2(\mu_3\text{-}OH)(BPT)_3]_n$ bilayer (Fig. S5†). The bilayers are further expanded by the 1,3-bimb ligands to form a 3D framework (Fig. 2c). The Co···Co distances separated by $\mu_6\text{-}BPT^{3-}$ are 14.632, 14.540 and 14.051 Å.

From the viewpoint of structural topology, the whole structure of complex **2** can be defined as a binodal (3,10)-connected 3,10T9 topology with the short Schläfli symbol $(4^{18}\cdot6^{24}\cdot8^3)_2$ by denoting the $[Co_4(\mu_3\text{-}OH)_2]^{6+}$ tetrameric SBUs as ten-connected nodes and BPT^{3-} ligands as three-connected nodes (Fig. 2d).

Structure descriptions of $\{[Zn(HBPT)(1,3\text{-bimb})]\cdot H_2O\}_n$ (3)

The single-crystal X-ray diffraction analysis reveals that complex **3** crystallizes in the triclinic system, $P\bar{1}$ space group. As shown in Fig. 3a, there is one Zn^{II} ion, one partly deprotonated $HBPT^{2-}$ ligand, one 1,3-bimb ligand, and one lattice water molecule in the asymmetric unit. Zn(1) is tetra-coordinated, completed by two oxygen atoms from two different $HBPT^{2-}$ ligands [Zn(1)–O(1) = 1.963(3) and Zn(1)–O(5B) = 1.964(2) Å] and two nitrogen atoms from two individual 1,3-bimb ligands [Zn(1)–N(1) = 2.046(3) and Zn(1)–N(4A) = 2.048(3) Å], resulting in a distorted tetrahedral coordination geometry. The bond angles around the Zn^{II} cation range from 94.28(12) to 123.15(12)°.

The H_3BPT ligands in complex **3** are partly deprotonated and exhibit a $(\kappa^1\text{-}\kappa^0)\text{-}(\kappa^1\text{-}\kappa^0)\text{-}\mu_2$ coordination mode (Mode III). Each $HBPT^{2-}$ ligand is connected to two Zn^{II} ions to form a 1D straight $[Zn(HBPT)]_n$ chain. Two neighbouring chains are linked *via* two bent 1,3-bimb ligands to form a 1D tube-like chain consisting of rhombus $[Zn_2(1,3\text{-bimb})_2]$ metallamacrocycles (Fig. 3b). The adjacent tube-like chains interacted with each other through O–H···π [O4–H4w···π = 3.794(0) Å], resulting in a supramolecular architecture (Fig. 3c).

Structure descriptions of $\{[Co_2(BPT)(H_2BPT)(4,4'\text{-bibp})_2]\cdot 2H_2O\}_n$ (4)

Structure analysis reveals that complex **4** crystallizes in the monoclinic system, $P2_1$ space group. As shown in Fig. 4a, the asymmetric unit consists of two Co^{II} ions, one BPT^{3-} ligand, one partly deprotonated H_2BPT^- ligand, two 4,4′-bibp ligands, and two lattice water molecules. Both Co(1) and Co(2) are penta-coordinated by three oxygen atoms from one BPT^{3-} ligand and one H_2BPT^- ligand and two nitrogen atoms from two 4,4′-bibp ligands. The bond lengths of Co–O and Co–N are in the range of 1.990(2)–2.104(2) and 2.072(3)–2.123(3) Å, respectively.

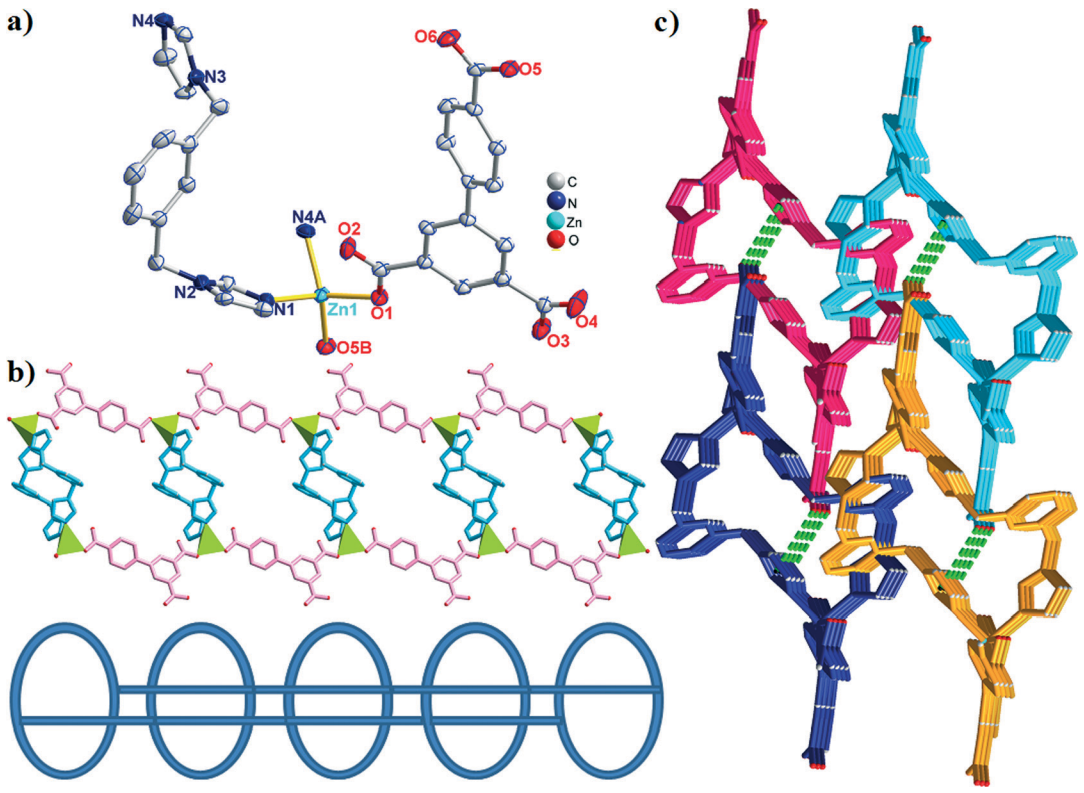

Fig. 3 (a) ORTEP representation of **3** with 50% thermal ellipsoid probability. Hydrogen atoms are omitted for clarity. Symmetry codes: A: $-x$, $2-y$, $2-z$; B: $1+x$, $1+y$, z. (b) Schematic view of the 1D tube-like chain and topology. (c) The 3D supramolecule connected through O–H···π interactions.

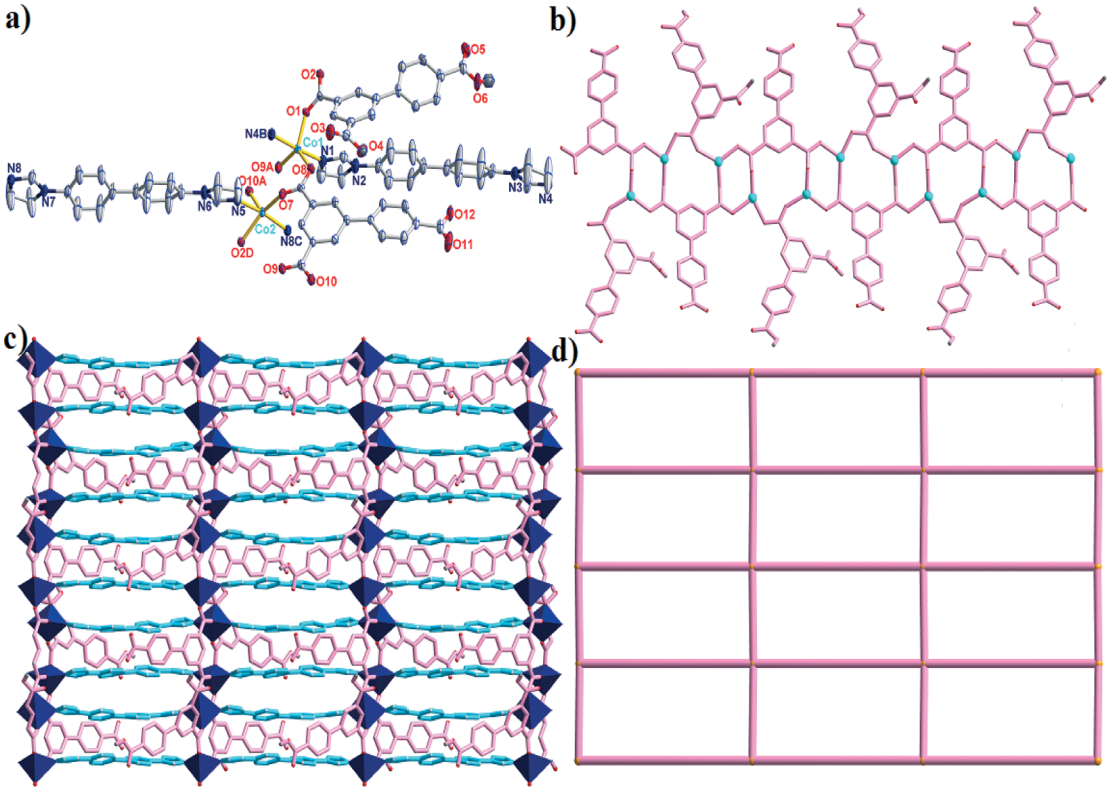

Fig. 4 (a) ORTEP representation of **4** with 50% thermal ellipsoid probability. Hydrogen atoms are omitted for clarity. Symmetry codes: A: 2 − *x*, −0.5 + *y*, 2 − *z*; B: 1 + *x*, *y*, 1 + *z*; C: −1 + *x*, *y*, −1 + *z*. (b) The 1D $[Co_2(BPT)(H_2BPT)]_n$ ladder chain. (c) The 2D networks constructed by the 1D chains sharing the $[Co_2(COO)_2]$ SBUs. (d) The $(4^4{\cdot}6^2)$-sql topology of the 2D nets in **4**.

The BPT^{3-} ligand exhibits two kinds of novel coordination modes in the assembly of complex **4**: the partly deprotonated one exhibits a $(\kappa^1\text{-}\kappa^1)\text{-}\mu_2$ coordination mode (Mode IV), and the completely deprotonated one displays a $(\kappa^0\text{-}\kappa^0)\text{-}(\kappa^1\text{-}\kappa^1)\text{-}(\kappa^1\text{-}\kappa^1)\text{-}\mu_4$ coordination mode (Mode V). Co^{II} ions are coordinated by BPT^{3-} and $HBPT^{2-}$ in staggered form, forming a $[Co_2(COO)_2]$ SBU based 1D ladder chain with the Co⋯Co distances being 3.965, and 4.682 Å, respectively (Fig. 4b). Along the *c* axis, the 1D chains are linked by 4,4′-bibp ligands, resulting in a 2D network (Fig. 4c). Topology analysis reveals that the whole structure can be viewed as a $(4^4{\cdot}6^2)$-sql net by denoting the $[Co_2(COO)_2]$ SBUs as 4-connected nodes (Fig. 4d).

Structure descriptions of $[Mn_{2.5}(BPT)(4,4'\text{-bibp})_{2.5}(SO_4)(H_2O)]_n$ (5)

A similar reaction environment to **4**, except for $MnSO_4{\cdot}H_2O$ replacing $Co(NO_3){\cdot}6H_2O$, results in one 3D 6-connected pcu framework. Structure analysis reveals that complex **5** crystallizes in the triclinic system, space group $P\bar{1}$. The asymmetric unit of **5** contains two and a half of Mn^{II} ions, one BPT^{3-} ligand, two and a half of 4,4′-bibp ligands, one SO_4^{2-} anion, and one coordinated water molecule as shown in Fig. 5a. Mn(1) is hexa-coordinated, completed by four oxygen atoms from two different BPT^{3-} ligands and two SO_4^{2-} anions and two nitrogen atoms from two individual 4,4′-bibp ligands, resulting in a distorted octahedral coordination geometry. Mn(2) is coordinated by two oxygen atoms from two BPT^{3-} ligands, one oxygen atom from a SO_4^{2-} anion, one associated water molecule, and two nitrogen atoms from two 4,4′-bibp ligands. Mn(3) is coordinated by two oxygen atoms from two BPT^{3-} ligands, another two oxygen atoms from one SO_4^{2-} anion, and two nitrogen atoms from two 4,4′-bibp ligands. The bond lengths of Mn–O and Mn–N are in the range of 2.120(2)–2.3326(19) and 2.220(3)–2.304(2) Å, respectively.

The BPT^{3-} ligand in complex **5** is completely deprotonated and exhibits a $(\kappa^1\text{-}\kappa^0)\text{-}(\kappa^1\text{-}\kappa^1)\text{-}(\kappa^1\text{-}\kappa^1)\text{-}\mu_5$ coordination mode (Mode VI). Mn^{II} cations are bridged by $(\kappa^1\text{-}\kappa^1)\text{-}\mu_2$ carboxylate groups and μ_3- SO_4^{2-} anions to generate a 2D network consisting of unprecedented pentanuclear $[Mn_5(COO)_6(SO_4)_2]$ SBUs with Mn⋯Mn distances being 4.053 Å (for Mn1–Mn3), 3.902 Å (for Mn2–Mn3), and 6.774 Å (for Mn1–Mn2) (Fig. 5b, S6†). The networks are further linked by two 4,4′-bibp ligands to result in a 3D framework (Fig. 5c).

From the viewpoint of structural topology, the whole 3D structure exhibits a 6-connected pcu net with α-Po primitive cubic nets with the short point symbol $(4^{12}{\cdot}6^3)$ by denoting $[Mn_5(COO)_6(SO_4)_2]$ SBUs as 6-connected nodes (Fig. 5d).

The diverse coordination modes of H_3BPT and the structural comparison

As shown in Scheme 3 and Table 2, H_3BPT exhibits versatile coordination modes, resulting in different new topologies. In complex **1**, H_3BPT is completely deprotonated and

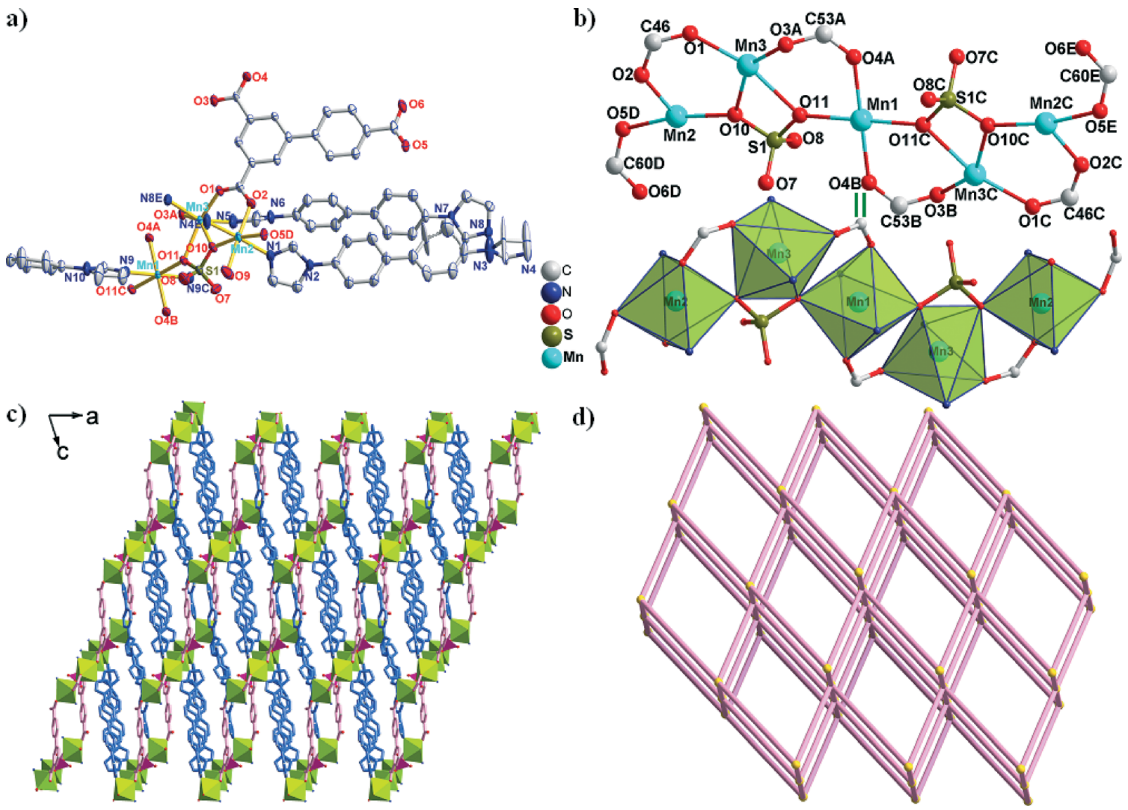

Fig. 5 (a) ORTEP representation of **5** with 50% thermal ellipsoid probability. Hydrogen atoms are omitted for clarity. Symmetry codes: A: 1 − *x*, 2 − *y*, 1 − *z*; B: *x*, −1 + *y*, *z*; C: 1 − *x*, 1 − *y*, 1 − *z*; D: −*x*, 2 − *y*, 2 − *z*; E: *x*, *y*, 1 − *z*. (b) The $[Mn_5(COO)_6(SO_4)_2]$ SBUs in compound **5**. (c) A perspective view of 3D frameworks viewed along the *b* axis. (d) The 3D 6-connected pcu-α-Po topology with the Schläfli symbol $(4^{12}\cdot6^3)$ in **5**.

Table 2 The coordination types of the H_3BPT ligand and the roles of ancillary ligands in complexes **1**–**5** and other ancillary ligand modified CPs[a]

Compound	Coord. modes	Ancillary ligands/role	Dihedral angles (°)	Structure and topology
1	Mode I	1,4-Bib/bridging + guest	20.27(1)	2D → 3D $(4^4\cdot5^4\cdot6^6\cdot8)(5\cdot6^4\cdot8)_2(5^2\cdot6^2)$ net
2	Mode II	1,3-Bimb/bridging	38.22(4)	3D (3,10)-connected $(4^{18}\cdot6^{24}\cdot8^3)(4^3)_2$ net
3	Mode III	1,3-Bimb/bridging	37.99(3)	1D tube-like chain
4	Mode IV/V	4,4′-Bibp/bridging	33.09(2)/16.20(8)	2D 4-connected $(4^4\cdot6^2)$ net
5	Mode VI	4,4′-Bibp/bridging	8.06(7)	3D 6-connected $(4^{12}\cdot6^3)$ net
$[Cd_3(BPT)_2(phen)_3]$[19a]	Mode VII	Phen/cheating	23.86(8)	1D → 2D interdigitated structure
$[Mn_5(HBPT)_4(phen)_4]$[19b]	Mode VIII/IX	Phen/cheating	28.69(1)/30.12(8)	2D 4-connected $(4^4\cdot6^2)$ net
$[Cd_2(BPT)(phen)_2]$[19b]	Mode X	Phen/cheating	37.06(3)	1D wave ladder chain
$[Cu_2(BPT)(phen)]$[19b]	Mode XI	Phen/cheating	8.61(1)	2D 3-connected $(4\cdot8^2)$ net
$[Mn(HBPT)_4(4,4'\text{-bipy})_{0.5}]$[19c]	Mode XI	4,4′-Bipy/bridging	34.05(0)	2D 4-connected $(4^4\cdot6^2)$ net
$[Cd(HBPT)(4,4'\text{-bipy})_{0.5}]$[19b]	Mode XI	4,4′-Bipy/bridging	34.95(1)	2D 4-connected $(4^4\cdot6^2)$ net
$[Co(HBPT)_4(4,4'\text{-bipy})_{0.5}]$[19c]	Mode XII	4,4′-Bipy/bridging	34.84(9)	2D 4-connected $(4^4\cdot6^2)$ net

[a] Note: all of the solvent molecules were omitted from the formulas. Abbreviation: phen = phenanthroline and 4,4′-bipy = 4,4′-bipyridine.

connects nickel ions *via* a $(\kappa^1\text{-}\kappa^1)\text{-}(\kappa^1\text{-}\kappa^0)\text{-}(\kappa^1\text{-}\kappa^0)\text{-}\mu_3$ coordination mode (Mode I), resulting in a ladder chain. The BPT^{3-} ligand in complex **2** exhibits a $(\kappa^1\text{-}\kappa^1)\text{-}(\kappa^1\text{-}\kappa^1)\text{-}(\kappa^0\text{-}\kappa^2)\text{-}\mu_6$ coordination mode (Mode II) and links Co^{II} into a 3D framework in the presence of 1,3-bimb ligands consisting of unreported $[Co_4(\mu_3\text{-}OH)_2]^{6+}$ tetrameric SBUs. With the help of 1,3-bimb ligands, Zn^{II} ions are coordinated by partly deprotonated H_2BPT^- ligands $((\kappa^1\text{-}\kappa^0)\text{-}(\kappa^1\text{-}\kappa^0)\text{-}\mu_2$, Mode III), resulting in a supramolecular architecture. H_3BPT exhibits two kinds of new coordination modes in **4**: a $(\kappa^1\text{-}\kappa^1)\text{-}\mu_2$ coordination mode (Mode IV) for the partly deprotonated one and $(\kappa^0\text{-}\kappa^0)\text{-}(\kappa^1\text{-}\kappa^1)\text{-}(\kappa^1\text{-}\kappa^1)\text{-}\mu_4$ for the completely deprotonated one (Mode V). Co^{II} ions are linked together to form one 2D structure. In **5**, BPT^{3-} exhibits a $(\kappa^1\text{-}\kappa^0)\text{-}(\kappa^1\text{-}\kappa^1)\text{-}(\kappa^1\text{-}\kappa^1)\text{-}\mu_5$ coordination mode to link Mn^{II} cations into a 3D framework containing 1D double helix chains. To the best of our knowledge, Modes II, IV, and V have never been documented up to now. As shown in the Scheme 3 and Table 2, six other kinds of coordination modes of H_3BPT (Modes VII–XII) in the presence of phenanthroline (phen) and 4,4′-bipyridine (4,4′-bipy) were reported.[19] The

results proved that the ancillary ligands have a great effect on the coordination modes of the host polycarboxylate aromatic acid and the final packing structures. The bis(imidazole) bridging linkers have an advantage over other N-donors since they can modulate their conformations and coordination modes to satisfy the coordination geometry of metal centers or metal clusters, resulting in an interpenetrated and high-dimensional architecture.

Thermal analyses

The experiments of thermogravimetric analysis (TGA) were performed on samples of **1**–**5** under a N_2 atmosphere with a heating rate of 10 °C min^{-1} as shown in Fig. S7.† For **1**, the first weight loss in the temperature range of 80–120 °C is consistent with the removal of the coordinated and lattice water molecules (obsd 5.4%, calcd 5.7%). The second weight loss of 16.8% (calcd: 17.2%) at *ca.* 150 °C corresponds to the loss of the guest molecule, 1,4-bib. Then the anhydrous network starts to collapse above 275 °C. For **2**, an initial weight loss of 2.4% corresponds to the loss of solvent water molecules (calcd: 2.6%). The second weight loss corresponds to the loss of the organic ligands. For **3**, the first weight loss from 80 to 110 °C is attributed to the loss of lattice water molecules (obsd 2.9%, calcd 3.0%). Above 290 °C, it starts to lose its ligands as a result of thermal decomposition. For **4**, the loss of lattice water molecules (obsd 3.1%, calcd 2.8%) is observed below 150 °C. The weight loss corresponding to the release of organic ligands is observed above 310 °C. For **5**, the weight loss of water molecules is observed in the range of 95–125 °C (obsd: 1.9% and calcd: 1.4%). The decomposition of organic ligands began at 295 °C.

Magnetic properties

The variable-temperature magnetic susceptibility measurements of **2**, **4**, and **5** were performed in the temperature range of 2–300 K under a field of 1000 Oe. The temperature dependence of $\chi_M T$ and χ_M^{-1} are displayed in Fig. 6 and 7.

The $\chi_M T$ value for **2** at room temperature is 5.75 cm^3 K mol^{-1}, lower than the theoretical one (7.48 cm^3 K mol^{-1}) for four high-spin Co(II) ions (S = 3/2) which can be attributed to the susceptible contribution from the orbital angular momentum at higher temperatures, indicating the overall antiferromagnetic coupling.[20] The $\chi_M T$ value for **4** at room temperature is 3.74 cm^3 K mol^{-1}, slightly lower than the value expected for two isolated high-spin Co(II) ions (3.75 cm^3 K mol^{-1}). With the temperature decreasing, the $\chi_M T$ value decreases evenly and the value of χ_M increases continuously. The above features all indicate overall antiferromagnetic coupling between Co(II) centers.[21] For **5**, the value for $\chi_M T$ at room temperature is 11.56 cm^3 K mol^{-1}, lower than the value for five isolated high-spin Mn(II) ions (21.87 cm^3 K mol^{-1}) which can be attributed to the susceptible contribution from the orbital angular momentum at higher temperatures, indicating the overall antiferromagnetic coupling.[22]

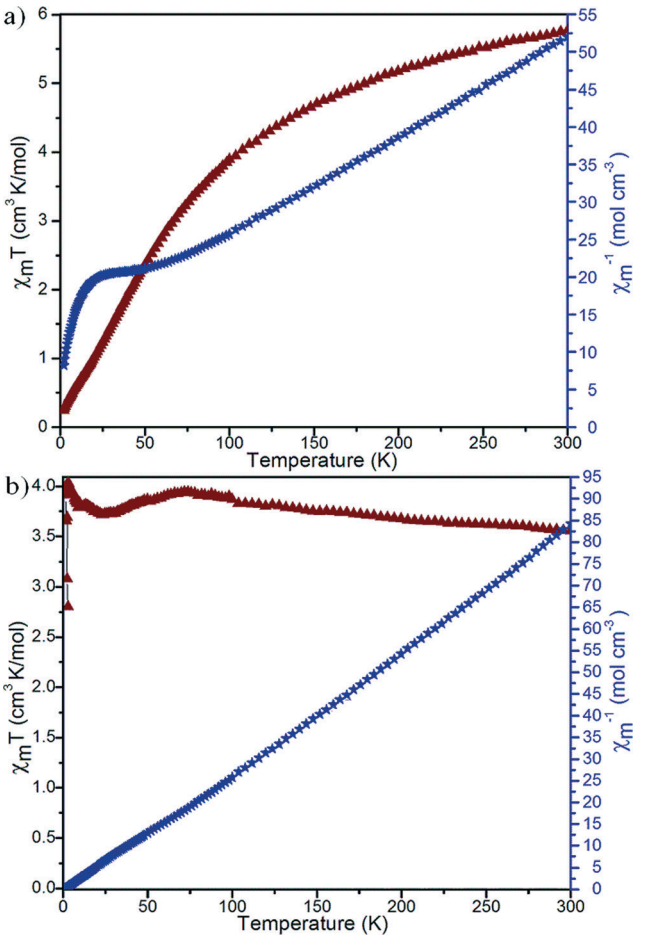

Fig. 6 The temperature dependence of magnetic susceptibilities of **2** (a) and **4** (b) under a static field of 1000 Oe.

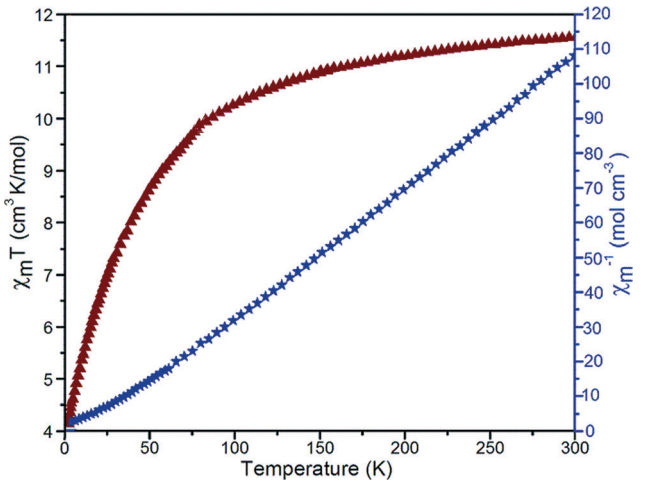

Fig. 7 The temperature dependence of magnetic susceptibilities of **5** under a static field of 1000 Oe.

Conclusions

In summary, five coordination polymers were synthesized based on biphenyl-3,4′,5-tricarboxylic acid (H_3BPT) and three

bis(imidazole) bridging linkers (1,4-bib, 1,3-bimb, and 4,4′-bibp) under hydrothermal conditions. Structural comparison of these networks reveals that the (bis)imidazole bridging ligands have a great effect on the coordination modes of H_3BPT, such as Modes II, IV, and V, which have never been documented to date. With the length of the (bis)imidazole ligands increasing, the longer separation of neighboring central ions makes the host aromatic polycarboxylate ligand adopt more "open" coordination modes and the overall structure a higher degree of interpenetration. The greater flexibility of ancillary ligands could make the final structure more twisted and complicated. Moreover, magnetic studies indicate that complexes **2**, **4**, and **5** have antiferromagnetic properties.

Notes

The authors declare no competing financial interest.

Acknowledgements

Financial support from the Natural Science Foundation of China (grant no. 21101097, 91022034 and 51172127), the Excellent Youth Foundation of Shandong Scientific Committee (Grant JQ201015), and the Qilu Normal University is acknowledged.

References

1 (*a*) G. Férey and C. Serre, *Chem. Soc. Rev.*, 2009, **38**, 1380; (*b*) B. L. Chen, N. W. Ockwig, A. R. Millward, D. S. Contreras and O. M. Yaghi, *Angew. Chem., Int. Ed.*, 2005, **44**, 4745; (*c*) J. Duan, Z. Yang, J. Bai, B. Zheng, Y. Li and S. Li, *Chem. Commun.*, 2012, **48**, 3058; (*d*) J. Duan, M. Higuchi, S. Horike, M. L. Foo, K. P. Rao, Y. Inubushi, T. Fukushima and S. Kitagawa, *Adv. Funct. Mater.*, 2013, **23**, 3525; (*e*) J. Duan, M. Higuchi, R. Krishna, T. Kiyonaga, Y. Tsutsumi, Y. Sato, Y. Kubota, M. Takata and S. Kitagawa, *Chem. Sci.*, 2014, **5**, 660.

2 (*a*) M. Kim, J. F. Cahill, H. Fei, K. A. Prather and S. M. Cohen, *J. Am. Chem. Soc.*, 2012, **134**, 18082; (*b*) H. Fei, J. F. Cahill, K. A. Prather and S. M. Cohen, *Inorg. Chem.*, 2013, **52**, 4011; (*c*) C. X. Chen, Q. K. Liu, J. P. Ma and Y. B. Dong, *J. Mater. Chem.*, 2012, **22**, 9027; (*d*) Y. Cui, Y. Yue, G. Qian and B. L. Chen, *Chem. Rev.*, 2012, **112**, 1126.

3 (*a*) D. Sun, S. Yuan, H. Wang, H. F. Lu, S. Y. Feng and D. F. Sun, *Chem. Commun.*, 2013, **49**, 6152; (*b*) B. X. Zhu, Q. L. Zhang, Y. Q. Zhang, Z. Tao, J. K. Clegg, J. R. Reimers, L. F. Lindoy and G. Wei, *Dalton Trans.*, 2009, 4896; (*c*) X. T. Zhang, L. M. Fan, X. Zhao, D. Sun, D. C. Li and J. M. Dou, *CrystEngComm*, 2012, **14**, 2053.

4 (*a*) F. Cao, S. Wang, D. Li, S. Zeng, M. Niu, Y. Song and J. Dou, *Inorg. Chem.*, 2013, **52**, 10747; (*b*) X. T. Zhang, D. Sun, B. Li, L. M. Fan, B. Li and P. H. Wei, *Cryst. Growth Des.*, 2012, **12**, 3845; (*c*) J. B. Lin, W. Xue, B. Y. Wang, J. Tao, W. X. Zhang, J. P. Zhang and X. M. Chen, *Inorg. Chem.*, 2012, **51**, 9423.

5 (*a*) X. Zhang, L. Fan, W. Zhang, Y. Ding, W. Fan and X. Zhao, *Dalton Trans.*, 2013, **42**, 16562; (*b*) X. J. Liang, X. D. Chen and J. C. Zhao, *Chem. Soc. Rev.*, 2014, **43**, 473; (*c*) H. Fu, Y. G. Li, Y. Liu, W. L. Chen, Q. Wu, J. X. Meng, X. L. Wang, Z. M. Zhang and E. B. Wang, *Cryst. Growth Des.*, 2011, **11**, 458; (*d*) W. Wang, J. Yang, W. Q. Kan and J. F. Ma, *CrystEngComm*, 2013, **15**, 5844.

6 (*a*) P. V. Dau and S. M. Cohen, *Chem. Commun.*, 2013, **49**, 6128; (*b*) Y. Wang, H. X. Lin, L. Chen, S. Y. Ding, Z. C. Lei, D. Y. Liu, X. Y. Cao, H. J. Liang, Y. B. Jiang and Z. Q. Tian, *Chem. Soc. Rev.*, 2014, **43**, 399.

7 (*a*) J. Duan, B. Zheng, J. Bai, Q. Zhang and Y. Zuo, *Inorg. Chim. Acta*, 2010, **363**, 3172; (*b*) L. M. Fan, X. T. Zhang, D. C. Li, D. Sun, W. Zhang and J. M. Dou, *CrystEngComm*, 2013, **15**, 349.

8 (*a*) F. F. B. J. Janssen, L. P. J. Veraart, J. M. M. Smits, R. D. Gelder and A. E. Rowen, *Cryst. Growth Des.*, 2011, **11**, 4313; (*b*) S. Banerjee, N. N. Adarsh and P. Dastidar, *Cryst. Growth Des.*, 2012, **12**, 6061.

9 (*a*) J. Li, L. Li, J. Liang, P. Cheng, J. Yu, Y. Xu and R. Xu, *Cryst. Growth Des.*, 2008, **8**, 2318; (*b*) S. Wang, R. Yun, Y. Peng, Q. Zhang, J. Lu, J. Dou, J. Bai, D. Li and D. Wang, *Cryst. Growth Des.*, 2012, **12**, 79.

10 (*a*) Q. Yu, Q. Zhang, H. Bian, H. Liang, B. Zhao, S. Yan and D. Liao, *Cryst. Growth Des.*, 2008, **8**, 1140; (*b*) Y. B. Wang, Y. L. Lei, S. H. Chi and Y. J. Luo, *Dalton Trans.*, 2013, **42**, 1862.

11 (*a*) W. Hong, H. Lee, T. H. Noh and O. S. Jung, *Dalton Trans.*, 2013, **42**, 11092; (*b*) C. Zhan, C. Zou, G. Q. Kong and C. D. Wu, *Cryst. Growth Des.*, 2013, **13**, 1429; (*c*) Q. L. Zhang, P. Hu, Y. Zhao, G. W. Feng, Y. Q. Zhang, B. X. Zhu and Z. Tao, *J. Solid State Chem.*, 2014, **210**, 178.

12 (*a*) Z. Wu, W. Sun, Y. Chai, W. Zhao, H. Wu, T. Shi and X. Yang, *CrystEngComm*, 2014, **16**, 406; (*b*) L. Ma, N. Yu, S. Chen and H. Deng, *CrystEngComm*, 2013, **15**, 1352; (*c*) F. Guo, B. Zhu, M. Liu, X. Zhang, J. Zhang and J. Zhao, *CrystEngComm*, 2013, **15**, 6191.

13 (*a*) P. V. Dau, K. K. Tanabe and S. M. Cohen, *Chem. Commun.*, 2013, **49**, 9370; (*b*) P. V. Dau, M. Kim and S. M. Cohen, *Chem. Sci.*, 2012, **4**, 601.

14 (*a*) A. G. Wong-Foy, O. Lebel and A. J. Matzger, *J. Am. Chem. Soc.*, 2007, **129**, 15740; (*b*) C. S. Lim, J. K. Schnobrich, A. G. Wong-Foy and A. J. Matzger, *Inorg. Chem.*, 2010, **49**, 5271.

15 (*a*) R. Singh and P. K. Bharadwaj, *Cryst. Growth Des.*, 2013, **13**, 3722; (*b*) X. T. Zhang, L. M. Fan, Z. Sun, W. Zhang, D. C. Li, J. M. Dou and L. Han, *Cryst. Growth Des.*, 2013, **13**, 792; (*c*) X. T. Zhang, L. M. Fan, W. Zhang, Y. S. Ding, W. L. Fan, L. M. Sun, X. Zhao and H. Lei, *Cryst. Growth Des.*, 2013, **13**, 2462; (*d*) L. Fan, X. Zhang, W. Zhang, Y. Ding, L. Sun, W. Fan and X. Zhao, *CrystEngComm*, 2014, **16**, 2144.

16 (*a*) G. M. Sheldrick, *SHELXTL, version 5.1*; Bruker Analytical X-ray Instruments Inc.: Madison, WI, 1998; (*b*) G. M. Sheldrick, *SHELX-97, PC Version*; University of Gottingen: Gottingen, Germany, 1997.

17 (*a*) V. A. Blatov, A. P. Shevchenko and V. N. Serezhkin, *J. Appl. Crystallogr.*, 2000, **33**, 1193; (*b*) The network topology was evaluated by the program "TOPOS-4.0", see: http://www.topos.ssu.samara.ru; (*c*) V. A. Blatov, M. O'Keeffe and D. M. Proserpio, *CrystEngComm*, 2010, **12**, 44.

18 (*a*) A. L. Spek, *J. Appl. Crystallogr.*, 2003, **36**, 7; (*b*) A. L. Spek, *PLATON, A Multipurpose Crystallographic Tool*, Utrecht University, Utrecht, The Netherlands, 2002.

19 (*a*) L. Li, J. Luo, S. Wang, Z. Sun, T. Chen and M. Hong, *Cryst. Growth Des.*, 2011, **11**, 3744; (*b*) Y. Lu, W. Zhao, Y. Liu, B. Liu, X. Feng, J. Tan and X. Yang, *J. Solid State Chem.*, 2012, **144**, 192; (*c*) C. C. Ji, J. Li, Y. Z. Li, Z. J. Guo and H. G. Zheng, *CrystEngComm*, 2011, **13**, 459.

20 (*a*) M. Ahmad, M. K. Sharma, R. Das, P. Poddar and P. K. Bharadwaj, *Cryst. Growth Des.*, 2012, **12**, 1571; (*b*) Q. Chen, W. Xue, J. B. Lin, R. B. Lin, M. H. Zeng and X. M. Chen, *Dalton Trans.*, 2012, **41**, 4199.

21 (*a*) H. Zhou, G. X. Liu, X. F. Wang and Y. Wang, *CrystEngComm*, 2013, **15**, 1377; (*b*) S. Y. Song, X. Z. Song, S. N. Zhao, C. Qin, S. Q. Su, M. Zhu, Z. M. Hao and H. J. Zhang, *Dalton Trans.*, 2012, **41**, 10412; (*c*) L. F. Ma, X. Q. Li, B. Liu, L. Y. Wang and H. W. Hou, *CrystEngComm*, 2011, **13**, 4973.

22 Y. Ma, K. Wang, E. Q. Gao and Y. Song, *Dalton Trans.*, 2010, **39**, 7714.